A&A 669, L13 (2023)
https://doi.org/10.1051/0004-6361/202245003

Astronomy & Astrophysics

LETTER TO THE EDITOR

A search for stellar tidal streams around Milky Way analogues from the SAGA sample

Juan Miró-Carretero[1], David Martínez-Delgado[3], Sílvia Farràs-Aloy[2,9], Maria A. Gómez-Flechoso[1,10], Andrew Cooper[4,5,11], Santi Roca-Fàbrega[1,6], Konrad Kuijken[9], Mohammad Akhlaghi[7], and Giuseppe Donatiello[8]

[1] Departamento de Física de la Tierra y Astrofísica, Universidad Complutense de Madrid, Plaza de las Ciencias, 28040 Madrid, Spain
e-mail: juamiro@ucm.es
[2] Universidad Internacional de Valencia (VIU), C. del Pintor Sorolla 21, 46002 Valencia, Spain
[3] Instituto de Astrofísica de Andalucía, CSIC, Glorieta de la Astronomía, 18080 Granada, Spain
[4] Institute of Astronomy and Department of Physics, National Tsing Hua University, Kuang Fu Rd. Sec. 2, Hsinchu 30013, Taiwan
[5] Center for Informatics and Computation in Astronomy, National Tsing Hua University, Kuang Fu Rd. Sec. 2, Hsinchu 30013, Taiwan
[6] Instituto de Astronomía, Universidad Nacional Autónoma de México, Apartado Postal 106, C. P. 22800, Ensenada, BC, Mexico
[7] Centro de Estudios de Física del Cosmos de Aragón (CEFCA), Plaza San Juan 1, 44001 Teruel, Spain
[8] UAI – Unione Astrofili Italiani /P.I. Sezione Nazionale di Ricerca Profondo Cielo, 72024 Oria, Italy
[9] Leiden Observatory, Leiden University, PO Box 9513, 2300, RA Leiden, The Netherlands
[10] Instituto de Física de Partículas y del Cosmos (IPARCOS), Fac. CC. Físicas, Universidad Complutense de Madrid, Plaza de las Ciencias, 1, 28040 Madrid, Spain
[11] Physics Division, National Center for Theoretical Sciences, Taipei 10617, Taiwan

Received 16 September 2022 / Accepted 29 December 2022

ABSTRACT

Context. Stellar tidal streams are the result of tidal interactions between a central galaxy and lower mass systems such as satellite galaxies or globular clusters. For the Local Group, many diffuse substructures have been identified and their link to the galaxy evolution has been traced. However, it cannot simply be assumed that the Milky Way or M 31 are representative of their galaxy class. Thus, a larger sample of analogue galaxies beyond the Local Group is required to bolster a broader generalisation of the underlying theory.

Aims. We want to detect and photometrically characterise stellar streams around Milky Way (MW-) analogues in the local Universe in order to extend the observational evidence of interactions between this class of host galaxies and their satellites. This information will be applicable in a more general context around future studies on galaxy formation and evolution processes.

Methods. In the present work, we identified and analysed stellar tidal streams around MW-analogue galaxies from the SAGA sample, using deep images of the DESI Legacy Imaging Surveys. For this sample, we obtained a range of *r*-band surface brightness limit between 27.8 and 29 mag arcsec^{-2}. We measured the surface brightness and colours of the detected streams using GNU Astronomy Utilities software.

Results. We identified 16 new stellar tidal streams around MW-analogue galaxies at distances between 25 and 40 Mpc. In applying a statistical analysis to our findings for the SAGA II galaxy sample, we obtained a frequency of 12.2% ± 2.4% for these stellar streams. We measured the surface brightness and colours of the detected streams and carried out a comparison to the dwarf satellite galaxies population around galaxies belonging to the same SAGA sample. We show that the mean colour of the streams is 0.20 mag redder than that of the SAGA satellites; in addition, the streams are, on average, 0.057 ± 0.021 mag redder that their progenitor (for cases where a likely progenitor could be identified).

Conclusions. The frequency of streams detected around MW-analogues in the Local Universe is in agreement with previous studies. The difference in colour between detected streams and satellites within the SAGA host galaxy sample could be explained by a combination of both selection biases in the SAGA study and physical processes.

Key words. galaxies: interactions – galaxies: dwarf – Galaxy: evolution – galaxies: photometry

1. Introduction

Over the last two decades, studies focused on the formation and evolution of our Galaxy have been significantly advanced by the first generation of wide-field, digital imaging surveys and the *Gaia* astrometric mission. The resulting extensive photometric databases have provided, for the first time, spectacular panoramic views of Milky Way tidal streams (Belokurov et al. 2006; Ibata et al. 2007, 2019; McConnachie et al. 2009; Shipp et al. 2018) and revealed the existence of large stellar sub-structures in the halo, which have been interpreted as observational evidence of our home Galaxy's hierarchical formation. Furthermore, the PAndAS survey (McConnachie et al. 2009) has revealed a panoramic view of the Andromeda halo with a multitude of tidal streams, arcs, shells, and other irregular structures that are possibly related to ancient merger events. These observations

confirm the ΛCDM prediction that tidally disrupted dwarf galaxies are important contributors to the formation of Galactic stellar halos. The next generation of Galactic and extragalactic surveys (e.g., LSST) will dissect the stellar halo structure of these Local Group spirals with unprecedented detail, promising further improvements in our understanding of the early formation and merger history of the Milky Way.

While some of the known stellar streams in the Milky Way and M 31 can be well characterised in a wide parameter space, also when including observations of their individual stars, the results for individual systems are not easily compared with numerical simulations due to the stochastic nature of galaxy assembly histories in the ΛCDM model. Although the statistical distributions, for example, of halo assembly times or satellite luminosities, are well defined for galaxies selected within a narrow range of stellar mass and/or halo mass, individual systems may show large deviations from the mean (Sotillo-Ramos et al. 2022). To overcome this limitation, a search for streams and other merger debris in a larger sample of Milky Way-like galaxies is required. This is a daunting task, as due to their extremely faint surface brightness, the observed frequency of stellar streams is very low, even in ultra-deep imaging surveys. For further details, we refer to Hood et al. (2018) for a modern review.

In this paper, we set our focus only on stellar tidal streams, arising from the tidal disruption of dwarf galaxies by more massive systems. We exploit the deep, wide-field imaging from the DESI Legacy Surveys (Dey et al. 2019) to systematically explore the frequency and photometric properties of streams in the stellar halos of 181 Milky Way analogue (MW-analogue) targets previously selected for the Satellites Around Galactic Analogs (SAGA) survey (Geha et al. 2017; Mao et al. 2021).

2. Methodology

2.1. Image sample

The SAGA survey's Stage I (Geha et al. 2017) and Stage II (Mao et al. 2021) define a parent sample of Milky Way-like host galaxies with absolute K-band magnitude in the range $-23 < M_K < -24.6$ mag, approximately equivalent to the stellar mass range $10^{10} < M_\star < 10^{11}\,M_\odot$. The sample is subject to environmental constrains by excluding close pairs of hosts, defined by a host-satellite K-band magnitude difference of $\Delta K < 1.6$ mag. The SAGA Stage I survey reports on 27 satellites around 8 MW-analogue hosts and Stage II, with an increased sample size, provides follow-up spectroscopy results for 127 satellites around 36 MW-analogue hosts. Here, we base our study on the SAGA II parent sample, including galaxies at distances $25 < d < 40.75$ Mpc. Further details of the SAGA Stage II parent sample can be found in Mao et al. (2021).

We inspected the images of the resulting sample of 181 galaxies using the Legacy Survey Sky Viewer[1] and selected a subset of targets for which stellar tidal streams could be identified by eye for further analysis. From this visual inspection, a total of 22 galaxies with detected streams were selected. Image cutouts of these selected targets were then computed from the raw data from the DESI Legacy Imaging Surveys (Dey et al. 2019; LS), using a modified version of the LS reduction pipeline Legacypipe. This alters the way the image backgrounds ("sky models") are computed. By default, this pipeline uses a flexible spline sky model which can oversubtract the outskirts of large galaxies. Instead, we subtracted the sky background from each CCD using a custom algorithm, which preserves the low-surface-brightness galactic features of interest. We first minimized the relative background levels between the overlapping CCDs in each band, and then, after detecting and masking sources as well as *Gaia* stars, we subtracted the sigma-clipped median in the outer half of the image cutout (see Martinez-Delgado et al. 2021 for details). In Appendix B, we describe the further processing of the images in order to measure the photometry parameters.

The resulting wide-field images reach surface brightness limits as faint as 29 mag arcsec^{-2} in the r band (see Sect. 2.2), ensuring a sufficient image depth to be able to measure very faint tidal structures. The images analysed in this work are listed in Table A.1. Examples of them are shown in Fig. 1.

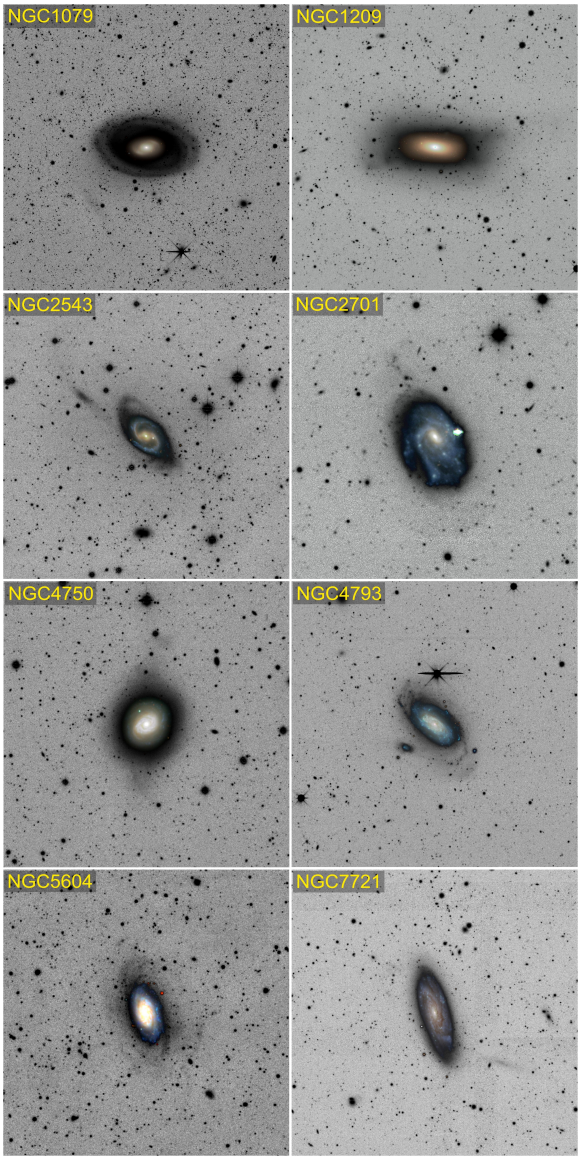

Fig. 1. Sample of images showing stellar streams around the galaxies listed in Table A.1. For the purposes of illustration, shallower colour images (also from the DESI Legacy Imaging Surveys) have been superimposed on the saturated central region of each host galaxy.

[1] https://www.legacysurvey.org/viewer

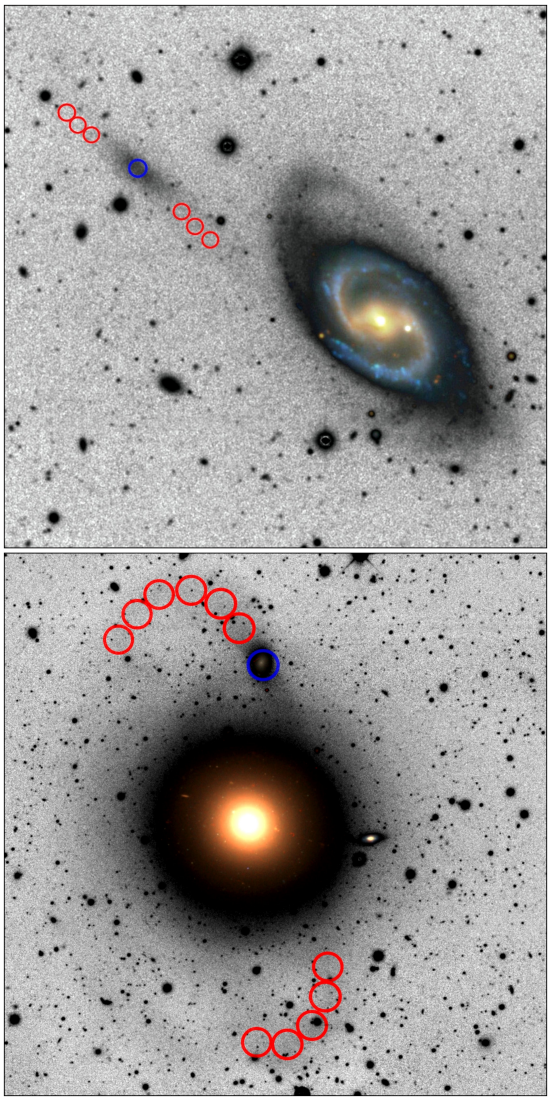

Fig. 2. Examples of our photometry measurement method, showing the apertures placed on the stellar streams around NGC 5812 and NGC 2543, along with the suspected progenitors, to measure their surface brightness and colours.

2.2. Data analysis

We carried out the photometric analysis with GNU Astronomy Utilities (Gnuastro)[2]. We made all the measurements by applying Gnuastro's MAKECATALOG subroutine on the sky-subtracted images generated by Gnuastro's NOISECHISEL (Akhlaghi & Ichikawa 2015; Akhlaghi 2019).

Our photometric analysis includes measurements of surface brightness in the LS r and g passbands for each stream, as well as for their candidate progenitor satellite (when identified). Taking advantage of the depth and photometric quality of the LS survey images, we also measured the $(g-r)_0$ colour of the streams. The progenitors are first tentatively identified by visual inspection, tracing apparent overdensities within the stream, and are then confirmed by measuring their colour $(g-r)_0$ and comparing it with the corresponding colour of the stream. This comparison, applied over many images in this and other works of the authors, has proven reliable in discriminating between stream-related overdensities and those that are not. We measured the surface brightness limit of the images for the g and r passbands following the approach of Román et al. (2020), that is, we report the value corresponding to $+3\sigma$ of the sky background in an area of 100 arcsec^2. Table A.1 reports the surface brightness limit for the r band. The images in this band are generally the ones with the largest detection area and are mostly free of stacking or reduction artifacts; they also provide a conservative, brighter limit value with regard to the g band.

We measured the surface brightness and colours on apertures placed manually on the stream, closely following the detection map of the stream generated by NOISECHISEL, once all foreground and background sources were masked. Regions where the stream surface brightness was judged to be significantly blended with light from the host galaxy were avoided. As an illustration of the method, Fig. 2 shows an example of a stream and the apertures on which the measurement of surface brightness and colour $(g-r)_0$ was performed. We obtained a representative surface brightness and colour for each stream by taking the mean of the individual aperture measurements. The method we followed to carry out the photometric analysis and estimating the errors, along with some important features of Gnuastro in the context of such an analysis, is explained in more detail in Appendix B.

3. Results

Table A.1 shows the results of our photometric analysis. We identified tidal streams around 22 galaxies from the sample of 181 MW-analogues. This suggests that $12.2\% \pm 2.4\%$ of the SAGA II galaxies have a stellar stream in the halo, for a r-band surface brightness limit range of our images between 27.8 and 29 mag arcsec^{-2} (see Table A.1). This implies that (with a 95% confidence level) the percentage of typical SAGA sample halos that have readily observable stellar streams is between 7.4% and 16.9%. These values correspond to the limits of the confidence interval for the proportion of a binomial distribution with a 95% confidence level. This result is similar to what was reported by Morales et al. (2018) for their systematic assessment of the frequency of tidal streams around a different sample of MW-like galaxies in the Local Universe. They reported a total of 28 tidal streams from a sample of 297 galaxies, providing a conservative estimate that only ~10% of galaxies show evidence of diffuse features that may be linked to satellite accretion events.

The measured ranges of stream surface brightness are $25.66 < \mu_g < 28.71$ and $25.23 < \mu_r < 27.98$ mag arcsec^{-2}. The detection significance index (DSI), as defined in Martinez-Delgado et al. (2021), is calculated by comparing the measurements for a given aperture with the median and standard deviation of N random measurements in pixels with no source detection[3]. The 'reference' column in Table A.1 indicates whether each stream has been previously reported in the literature or whether it is reported for the first time in this work.

Figure 3 compares the $(g-r)_0$ colour distribution of the stellar streams identified in Table A.1 (shown in red) to that of the 127 spectroscopically confirmed satellite galaxies from the 36 SAGA systems presented in Mao et al. (2021) (shown in blue). The hypothesis contrast of normality shows that the null hypothesis (which is that the colour distributions come from a Gaussian distribution) cannot be rejected with a 99% confidence level. We therefore fit Gaussian functions to each distribution,

[2] http://www.gnu.org/software/gnuastro

[3] https://www.gnu.org/software/gnuastro/manual/html_node/Upper-limit-magnitude-of-each-detection.html

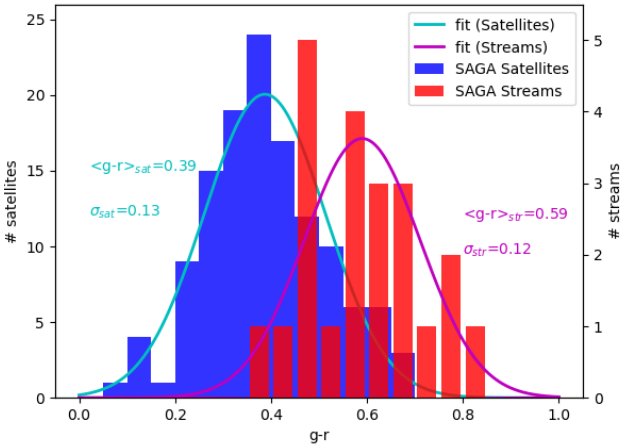

Fig. 3. Histogram showing the distribution of the average $(g - r)_0$ colour of stellar streams around 22 galaxies from our sample (listed in Table A.1), together with the same colour of the 127 satellite galaxies from the 36 SAGA systems sample.

finding means and standard deviations of 0.59 ± 0.12 mag for the streams and 0.39 ± 0.13 mag for the SAGA satellites. The mean colour of the streams is therefore 0.20 mag redder than that of the SAGA satellites. An equality of means hypothesis test shows that the null hypothesis can be rejected with a statistical confidence level larger than 99.999% (p-value $< 10^{-10}$) and the alternative hypothesis that mean colour of the streams is redder than the mean colour of satellites can be accepted. The $(g-r)_0$ colours we find are similar to those obtained for the streams described in the proof-of-concept study of Martinez-Delgado et al. (2021), who reported a mean and standard deviation of 0.66 ± 0.12 mag.

In approximately 36% of the streams in our sample, we have identified a highly likely progenitor by visual inspection. This allows us to explore similarities and differences in the stellar populations of satellites and their streams, including the presence of population gradients along the streams. As shown in Fig. 2 for the cases of NGC 2543 and NGC 5812, we placed apertures on the likely progenitors as well as along the tidal features. Table A.2 compares the $(g - r)_0$ colour of the stream (averaged over the apertures as described in Sect. 2.2) with that measured in an aperture placed on the suspected progenitor. We see a significant difference in colour for the streams around NGC 2543, NGC 4793, and NGC 5812, with the stream redder than its likely progenitor by 0.21, 0.16, and 0.14 mag, respectively. For the rest of streams where a progenitor is suspected, the colour difference is within the uncertainties of our colour measurement – and therefore is not significant. To test whether the differences observed in our sample are statistically significant or not, we performed a hypothesis test of the difference between the stream and the progenitor colours. Thus, we have obtained that streams are, on average, 0.057 ± 0.021 mag redder that their progenitor, with a confidence level of >99.99%.

4. Conclusions

The main conclusions of this study are as follows:

- We detected 16 previously unreported streams in MW-like host galaxies from the SAGA sample at distances between 25 and 40 Mpc (see Table A.1, column labelled 'reference').
- We measured the surface brightness and colours of 22 streams (including the new discoveries) in MW-like hosts of the same SAGA sample by analysing DESI Legacy Imaging Survey *grz* images with Gnuastro, a novel tool developed with emphasis on the detection of faint structures. The measured ranges of stream surface brightness are $25.66 < \mu_g < 28.71$ and $25.23 < \mu_r < 27.98$ mag arcsec^{-2}.
- We suggest the frequency of streams for the SAGA sample to be $12.2\% \pm 2.4\%$, for a r-band surface brightness limit range of our images between 27.8 and 29 mag arcsec^{-2}, in line with previous studies.
- We carried out a statistical comparison of $(g-r)_0$ colours for the detectable stream and satellite populations in our sample, finding that the typical colours of the streams we detected are significantly redder, on average.
- In those systems where a progenitor of the stream could be identified by visual inspection and photometric analysis of the images, we find the stream is on average slightly redder than the progenitor.

We suggest that the differences we find between the stream and satellite colour distributions may be explained by a combination of selection bias and physical effects. Here, we provide a brief summary of possible explanations. We defer a more detailed discussion that is outside of the scope of this Letter to follow-up works.

The SAGA survey offers a sample of candidate satellites based on catalogue photometry and follows up on a subset of these with multi-object fibre spectrographs to obtain redshifts. Extremely compact (M 32-like) candidates did not receive such a follow-up (Geha et al. 2017) and, although such objects tend to be red, relatively few are known. More significantly, as reported in Mao et al. (2021), following from Fig. 6, redshifts are more difficult to obtain for candidates with a low mean-surface-brightness, which also tend to be redder. More generally, in the regime of satellite dwarf galaxies, both surface brightness and colour are (broadly) correlated with total luminosity. At a fixed size, the most luminous objects (and hence those with a higher surface brightness) tend to be those that are star-forming, or at least relatively younger. This naturally makes them bluer. Mao et al. (2021) argue that this redshift incompleteness is a weak effect that does not significantly bias the distribution of star formation rates (i.e., colours) in the spectroscopic sample. However, the completeness of the initial target catalogue may also be important. Font et al. (2022) explore this issue in detail through comparison to the RTEMIS suite of cosmological simulations. They suggest that the photometric SAGA candidate sample may have a significant bias against low-surface-brightness satellites and that this bias has a much stronger effect on the resulting colour distribution. Font et al. (2022) speculate that this bias arises from the effect mentioned above: recently-accreted star-forming satellites have a higher surface brightness than their redder counterparts at fixed luminosity, and are therefore more likely to be targeted by SAGA (and more likely to have a successful redshift if observed). For example, we refer to Fig. 2 in Font et al. (2022), which shows the separation between star forming satellites with high surface brightness and quenched satellites at similar magnitudes with lower surface brightness. In making a comparison to a separate survey of satellites in the Local Volume (Exploration of Local VolumE Satellites, ELVES, see Carlsten et al. 2021), they find evidence that fainter galaxies in SAGA are biased towards bluer colours.

However, even with the small sample of stream colours presently available, we find at least two reasons to consider physical explanations for the colour differences in addition to selection effects. First, Font et al. (2022) find the potential

selection bias in SAGA mostly affects the fainter satellite magnitudes ($M_V > -12$), and that the colours of brighter (systematically bluer) satellites are not strongly biased. Although we cannot yet quantify the total luminosity of the streams in our sample, it is likely that readily detectable streams have some bias towards the brighter end of the luminosity function of disrupted progenitors (albeit with large uncertainty due to the wide variety of stream morphology and viewing angle). If we were to compare the streams only to the brighter SAGA satellites, rather than the full sample, the discrepancy in colour would be reinforced. Put another way, we detect no streams as blue as the bluest SAGA satellites.

Secondly, the difference in colour seen in the small number of stream-progenitor pairs in our sample suggests colour gradients may contribute alongside selection-driven differences between the stream and satellite samples (and other population-level effects, such as different average ages). Such gradients may be established either before disruption or during the disruption process. A wide variety of physical processes could create gradients through their effects on the relative timescales of gas removal (due to ejection and ram pressure stripping), star formation in residual cold gas, and tidal stripping. At the most basic level, complete tidal disruption will prevent further star formation, leading to the systematic reddening of dynamically older streams. Cosmological simulations are necessary to make quantitative predictions for colour distributions, accounting for the range of satellite star formation histories, gas fractions and orbits, and variations in the satellite accretion rate and disruption efficiency over the range of dark matter halo masses that may correspond to the SAGA sample.

To make further progress, we are currently constructing a larger sample of galaxies within the Stellar Streams Legacy Survey (Martinez-Delgado et al. 2021). This sample will comprise more than 800 Milky Way-like galaxies. By analysing this sample using the techniques presented in this paper, we will be able to more robustly test our conclusions and carry out meaningful comparisons to physical models of satellite star formation, accretion and disruption.

Acknowledgements. We want to thank to Yao-Yuan Mao, Marla Geha and Risa Wechsler for providing the original SAGA sample for this paper and useful comments. We also thank Dustin Lang and John Moustakas for running the modified Legacypipe code to produce the images used here. DMD acknowledges financial support from the Talentia Senior Program (through the incentive ASE-136) from Secretaría General de Universidades, Investigación y Tecnología, de la Junta de Andalucía. DMD acknowledges funding from the State Agency for Research of the Spanish MCIU through the "Center of Excellence Severo Ochoa" award to the Instituto de Astrofísica de Andalucía (SEV-2017-0709) and project (PDI2020-114581GB-C21/ AEI / 10.13039/501100011033). MAGF acknowledges financial support from the Spanish Ministry of Science and Innovation through the project PID2020-114581GB-C22. SRF acknowledges financial support from the Spanish Ministry of Economy and Competitiveness (MINECO) under grant number AYA2016-75808-R, AYA2017-90589-REDT and S2018/NMT-429, and from the CAM-UCM under grant number PR65/19-22462. SRF acknowledges support from a Spanish postdoctoral fellowship, under grant number 2017-T2/TIC-5592. APC is supported by the Taiwan Ministry of Education Yushan Fellowship and Taiwan National Science and Technology Council grant 109-2112-M-007-011-MY3. The photometry analysis in this work was partly done using GNU Astronomy Utilities (Gnuastro, ascl.net/1801.009) version 0.17. Work on Gnuastro has been funded by the Japanese MEXT scholarship and its Grant-in-Aid for Scientific Research (21244012, 24253003), the European Research Council (ERC) advanced grant 339659-MUSICOS, and from the Spanish Ministry of Economy and Competitiveness (MINECO) under grant number AYA2016-76219-P. The Leiden Observatory has provided facilities and computer infrastructure for carrying out part of this work. MA acknowledges the financial support from the Spanish Ministry of Science and Innovation and the European Union - NextGenerationEU through the Recovery and Resilience Facility project ICTS-MRR-2021-03-CEFCA.

References

Akhlaghi, M. 2019, ASP Conf. Ser., 521, 299A
Akhlaghi, M., & Ichikawa, T. 2015, ApJS, 220, 1
Belokurov, V., Zucker, D. B., Evans, N. W., et al. 2006, ApJ, 642, L137
Carlsten, S. G., Greene, J. E., Greco, J. P., et al. 2021, ApJ, 922, 267
Dey, A., Schlegel, D. J., Lang, D., et al. 2019, AJ, 157, 168
Font, A. S., McCarthy, I. G., Belokurov, V., et al. 2022, MNRAS, 511, 1544
Geha, M., Wechsler, R. H., Mao, Y.-Y., et al. 2017, ApJ, 847, 4
Hood, C. E., Kannappan, S. J., Stark, D. V., et al. 2018, ApJ, 857, 144
Ibata, R., Martin, N. F., Irwin, M., et al. 2007, ApJ, 671, 1591
Ibata, R., Malhan, K., & Martin, N. 2019, ApJ, 872, 152
Knierman, K. A., Scowen, P., Veach, T., et al. 2013, ApJ, 774, 125
Ludwig, J. 2014, PhD Thesis, Universität Heidelberg, Germany
Mao, Y.-Y., Geha, M., Wechsler, R. H., et al. 2021, ApJ, 907, 85
Martinez-Delgado, D., Cooper, A. P., Roman, J., et al. 2021, A&A, in press https://doi.org/10.1051/0004-6361/202245011
McConnachie, A. W., Irwin, M. J., Ibata, R. A., et al. 2009, Nature, 461, 66
Miskolczi, A., Bomans, D. J., & Dettmar, R.-J. 2011, A&A, 536, A66
Morales, G., Martínez-Delgado, D., Grebel, E. K., et al. 2018, A&A, 614, A143
Román, J., Trujillo, I., & Montes, M. 2020, A&A, 644, A42
Shipp, N., Drlica-Wagner, A., Balbinot, E., et al. 2018, ApJ, 862, 114
Sotillo-Ramos, D., Pillepich, A., Donnari, M., et al. 2022, MNRAS, 516, 5404

Appendix A: Tables

Table A.1. Photometry of stellar streams around MW analogue galaxies.

Host	D	$\mu_{r,limit}$	DSI_{stream}		$\langle\mu_g\rangle_{stream}$	$\langle\mu_r\rangle_{stream}$	$\langle(g-r)_0\rangle_{stream}$	Reference
			maximum	average				
	Mpc	[mag arcsec^{-2}]	σ	σ	[mag arcsec^{-2}]	[mag arcsec^{-2}]	[mag]	
NGC 0636	29.2	28.88	45.58	31.86	26.66 ± 0.03	25.86 ± 0.02	0.75 ± 0.04	(∗)
NGC 1079	31.4	28.78	15.24	11.31	27.51 ± 0.05	27.00 ± 0.05	0.48 ± 0.07	(∗)
NGC 1209	38.3	28.91	8.85	4.71	28.71 ± 0.05	27.98 ± 0.03	0.68 ± 0.07	(∗)
NGC 1309	34.3	28.76	24.42	23.02	26.26 ± 0.02	25.66 ± 0.02	0.56 ± 0.02	(1)
NGC 2460	34.8	28.81	10.39	8.06	27.50 ± 0.05	26.57 ± 0.04	0.85 ± 0.06	(3)
NGC 2543	37.6	28.55	10.18	9.00	26.66 ± 0.06	25.86 ± 0.06	0.72 ± 0.08	(∗)
NGC 2648	32.7	28.19	22.70	16.62	26.49 ± 0.03	25.96 ± 0.04	0.49 ± 0.05	(∗)
NGC 2701	36.5	28.58	6.63	5.55	26.85 ± 0.07	26.47 ± 0.08	0.37 ± 0.10	(∗)
NGC 2782	39.9	28.51	28.69	20.55	26.14 ± 0.01	25.63 ± 0.02	0.48 ± 0.02	(4)
NGC 3614	36.1	28.57	9.79	6.64	27.78 ± 0.06	27.07 ± 0.05	0.68 ± 0.08	(∗)
NGC 3689	39.8	28.00	10.75	6.45	27.55 ± 0.05	26.82 ± 0.05	0.56 ± 0.07	(1)
NGC 4378	37.2	28.21	24.06	22.17	27.24 ± 0.03	26.53 ± 0.03	0.68 ± 0.04	(∗)
NGC 4750	27.7	28.57	54.58	35.07	26.81 ± 0.02	26.30 ± 0.03	0.48 ± 0.03	(∗)
NGC 4793	36.3	28.11	20.02	18.04	26.16 ± 0.04	25.60 ± 0.06	0.55 ± 0.07	(∗)
NGC 4799	40.1	27.93	8.49	6.98	26.65 ± 0.04	26.20 ± 0.07	0.41 ± 0.08	(∗)
NGC 5297	35.5	28.55	28.00	18.58	26.35 ± 0.04	25.70 ± 0.04	0.63 ± 0.05	(∗)
NGC 5493	40.05	28.30	32.96	28.06	26.38 ± 0.02	25.69 ± 0.02	0.63 ± 0.003	(∗)
NGC 5604	39.0	28.18	12.29	9.93	26.35 ± 0.05	25.81 ± 0.05	0.46 ± 0.07	(∗)
NGC 5631	31.7	28.54	12.88	10.01	27.60 ± 0.04	26.98 ± 0.04	0.59 ± 0.06	(∗)
NGC 5750	25.3	28.23	29.41	27.37	27.38 ± 0.05	26.69 ± 0.04	0.63 ± 0.06	(2)
NGC 5812	27.2	28.38	55.09	30.73	26.54 ± 0.03	25.67 ± 0.02	0.77 ± 0.04	(∗)
NGC 7721	31.8	27.87	19.44	13.24	25.79 ± 0.03	25.23 ± 0.04	0.53 ± 0.05	(3)

Notes. Column 1 gives the name of the host galaxy and Col. 2 its distance. Column 3 shows the surface brightness limit in the r band calculated in this work. Note: the image surface brightness limit is in itself the 3σ value of the sky surface brightness measured in the non-detection zone of the image and extrapolated to an aperture of 100 arcsec^2; the standard deviation of the sky background value across the image is within 0.1 mag arcsec^{-2} for most of the images, in a few cases being between 0.1 and 0.2 mag arcsec^{-2}. Columns 4 and 5 show the detection significance index, as defined in Martinez-Delgado et al. (2021). Cols. 6–8 show the surface brightness in the g passband, in the r passband, and the $(g-r)_0$ colour of the streams, averaged over all the apertures placed on the stream; Col. 9 indicates whether the stream has been reported for the first time in this work, indicated by (∗), or in one of the following previous works: (1) Martinez-Delgado et al. (2021); (2) Morales et al. (2018); (3) Ludwig (2014); (4) Knierman et al. (2013).

Table A.2. Comparison between the average $(g-r)_0$ colour of each stream and the corresponding colour of its visually identified progenitor.

Host	$\langle(g-r)_0\rangle_{stream}$ [mag]	$\langle(g-r)_0\rangle_{progenitor}$ [mag]	Δ [mag]
NGC 2543	0.72 ± 0.08	0.51 ± 0.02	0.21 ± 0.08
NGC 2648	0.49 ± 0.05	0.56 ± 0.003	−0.07 ± 0.05
NGC 3614	0.68 ± 0.08	0.65 ± 0.08	0.03 ± 0.11
NGC 3689	0.56 ± 0.07	0.59 ± 0.02	−0.03 ± 0.07
NGC 4793	0.55 ± 0.07	0.39 ± 0.01	0.16 ± 0.07
NGC 5297	0.63 ± 0.05	0.64 ± 0.004	−0.01 ± 0.05
NGC 5750	0.63 ± 0.06	0.57 ± 0.02	0.06 ± 0.06
NGC 5812	0.77 ± 0.04	0.63 ± 0.005	0.14 ± 0.04

Appendix B: Photometry Measurement Method

For the detection of the streams (and all other sources of the images), we use NoiseChisel, part of the state-of-the-art Gnuastro software, designed specifically to detect low-surface-brightness structures. NoiseChisel also calculates the background sky and subtracts it from the input image. The subtracted background sky level is not a constant value over the image; the sky is assumed to be constant only on tiles of a configurable number of pixels (typically 40x40), which form a tessellation of many tiles over the image. In this way, the environment of the stream is taken into consideration for the calculation of the sky background to be subtracted locally. For a complete introduction to the robustness of this method, we refer to the corresponding chapter of the Gnuastro book [4]. Then, segmentation is carried out by Gnuastro's Segment package, which labels all the sources detected. The foreground and background sources are identified as clumps and are masked before the photometry measurements are carried out by MakeCatalog, another package belonging to Gnuastro.

Regarding the modelling and subtraction of the host galaxy halo, this approach was applied earlier in this study by modelling the host halo with a Sersic profile. However, due to the irregular shape of the spiral host galaxies analysed, this technique was difficult to apply, particularly for hosts that are not face-on, and had the effect of over-subtracting the diffuse area around the host; this negatively impacted the photometry measurement of the stream. Instead, we actually estimated the zone of influence for every host by measuring the gradient of the surface brightness in its faint surroundings and masking the host to the point of transition to a flat gradient, making sure the apertures where the stream photometry is measured lie outside of such a zone. This is only relevant for those streams that are close to the outskirts of the host galaxy.

We measured the surface brightness and colours on apertures, placed manually following closely the detection map of the stream generated by NoiseChisel, once all foreground and background sources were masked. A succession of circular apertures allows to measure colour gradients and can easily adapt to the stream contour; however, in a few cases where the stream shape allowed, larger polygonal apertures were used to reduce the measurement error. Table B.1 shows the dimensions of the apertures for each stream. The diameter of the circular apertures is as close as possible to the perceived width of the stream. Regions where the stream surface brightness was judged to be significantly blended with light from the host galaxy or were significantly obscured by clumps were avoided.

Within each (circular or polygonal) aperture, the flux is measured over every pixel and then integrated. The integrated magnitude and the surface brightness measurements over the area of the aperture, are derived from the flux measurement. Table B.1 shows the average over all the apertures placed on the stream of the galactic extinction-corrected integrated magnitude for the bands g and r. The magnitude error is calculated with $M_{error} = 2.5 / S/N \ln(10)$ [5]; as the aperture area increases, the signal-to-noise ratio (S/N) also increases, so the magnitude error decreases. This is different from the flux error in each pixel (which increase with the square root of the area). However, signal increases linearly with area, so overall, the S/N increases as the area grows larger.

The colour $(g - r)_0$ is given for each aperture by the difference between the galactic extinction-corrected magnitudes in the respective bands g and r in that aperture. Then the colour $(g-r)_0$ of a stream (as given in Table A.1) is the average of that colour in all the apertures placed on the stream.

[4] https://www.gnu.org/software/gnuastro/manual/html_node/Skewness-caused-by-signal-and-its-measurement.html

[5] https://www.gnu.org/software/gnuastro/manual/html_node/Magnitude-measurement-error-of-each-detection.html

Table B.1. Names of stream hosts and their coordinates are shown in columns 1-3. Columns 4 and 5 show the average over all the apertures placed on the stream of the galactic extinction-corrected integrated magnitude for the bands g and r. Column 6 shows the number and the size of the apertures used to measure the photometric parameters.

Host	RA deg	DEC deg	$\langle g_0 \rangle_{\rm aperture}$ [mag]	$\langle r_0 \rangle_{\rm aperture}$ [mag]	Area arcsec^2
NGC0636	24.777227	-7.512649	20.53 ± 0.03	19.76 ± 0.02	18 × 304
NGC1079	40.934733	-29.003346	20.93 ± 0.05	20.44 ± 0.05	4 × 447
NGC1209	46.512529	-15.611249	19.55 ± 0.05	18.86 ± 0.03	3 × 4229
NGC1309	50.527313	-15.400056	19.66 ± 0.02	19.09 ± 0.02	3 × 461
NGC2460	119.21775	60.349361	21.26 ± 0.05	20.41 ± 0.04	5 × 333
NGC2543	123.241359	36.25462	22.10 ± 0.06	21.37 ± 0.06	4 × 59
NGC2648	130.665883	14.285559	20.07 ± 0.03	19.57 ± 0.04	2 × 372
NGC2701	134.773869	53.771657	22.03 ± 0.07	21.65 ± 0.08	6 × 75
NGC2782	138.521169	40.113726	19.22 ± 0.01	18.73 ± 0.02	15 × 609
NGC3614	169.588899	45.748213	21.15 ± 0.06	20.46 ± 0.05	6 × 470
NGC3689	172.046015	25.66108	19.93 ± 0.05	19.37 ± 0.05	1 × 877
NGC4378	186.325235	4.924945	19.45 ± 0.03	18.75 ± 0.03	2 × 1246
NGC4750	192.530041	72.874472	19.82 ± 0.02	19.34 ± 0.03	4 × 750
NGC4793	193.669165	28.938744	21.38 ± 0.04	20.82 ± 0.05	6 × 83
NGC4799	193.814721	2.896617	20.90 ± 0.04	20.48 ± 0.07	3 × 180
NGC5297	206.598645	43.872219	20.87 ± 0.04	20.23 ± 0.03	2 × 150
NGC5493	212.872404	-5.043581	19.95 ± 0.02	19.30 ± 0.02	7 × 379
NGC5604	216.178326	-3.212203	21.12 ± 0.05	20.65 ± 0.05	3 × 111
NGC5631	216.638694	56.582627	20.48 ± 0.04	19.88 ± 0.04	3 × 707
NGC5750	221.546359	-0.222971	19.97 ± 0.05	19.33 ± 0.04	3 × 849
NGC5812	225.232043	-7.457279	19.91 ± 0.03	19.13 ± 0.02	15 × 475
NGC7721	354.702194	-6.51799	20.27 ± 0.03	19.74 ± 0.04	1 × 146